Membranes Hot Paper

Deutsche Ausgabe: DOI: 10.1002/ange.201505663
Internationale Ausgabe: DOI: 10.1002/anie.201505663

Self-Assembled Asymmetric Block Copolymer Membranes: Bridging the Gap from Ultra- to Nanofiltration

*Haizhou Yu, Xiaoyan Qiu, Nicolas Moreno, Zengwei Ma, Victor Manuel Calo, Suzana P. Nunes, and Klaus-Viktor Peinemann**

Abstract: *The self-assembly of block copolymers is an emerging strategy to produce isoporous ultrafiltration membranes. However, thus far, it has not been possible to bridge the gap from ultra- to nanofiltration and decrease the pore size of self-assembled block copolymer membranes to below 5 nm without post-treatment. It is now reported that the self-assembly of blends of two chemically interacting copolymers can lead to highly porous membranes with pore diameters as small as 1.5 nm. The membrane containing an ultraporous, 60 nm thin separation layer can fully reject solutes with molecular weights of 600 g mol^{-1} in aqueous solutions with a water flux that is more than one order of magnitude higher than the permeance of commercial nanofiltration membranes. Simulations of the membrane formation process by dissipative particle dynamics (DPD) were used to explain the dramatic observed pore size reduction combined with an increase in water flux.*

Nanoporous membranes are an important tool for water softening, the removal of micropollutants, the demineralization of organic solutes, protein separation, and the recovery of dyes from waste water.[1,2] Although a wide variety of nanoporous membrane systems have been developed, a number of challenges in their production still exist.[3–6] These include improving the permeability of the membranes with simultaneous and efficient rejection of specific molecules, up-scaling the production process, reducing membrane fouling, and improving the reproducibility of the membrane performance. The self-assembly of well-defined block copolymers (BCPs) is a key strategy in the fabrication of functional nanostructured materials.[7,8] Amphiphilic BCPs are able to self-assemble into well-defined nanoscale structures with a domain spacing that depends on the balance of repulsive interactions between dissimilar segments and the conformational entropy loss of the distinct blocks.[9–11] Several years ago, Peinemann et al. reported a simple and scalable technique for fabricating integral asymmetric isoporous block copolymer membranes.[12] Since then, our group has studied the formation mechanism and tuned the pore size between 20 and 3 nm.[13–15] The sub-10 nm pores were obtained by electroless gold deposition.[13] However, according to the Hagen–Poiseuille equation,

$$dv/dt = (\pi R^4 \Delta p)/(8\eta L) \quad (1)$$

the flux (dv/dt) decreases rapidly as the pore radius decreases. To address this decrease in flux, we focused on the fabrication of nanoporous membranes with high water permeability by combining the self-assembly of AB/AC BCP blends with non-solvent-induced phase separation. We investigated the blending of BCPs because of the simplicity of the process.

Bulk morphologies, thin films, and micelles of BCP blends have been studied previously whereas only a few studies of such membranes have been conducted.[16–20] The most recent publication on blended BCP membranes describes the blends of two AB block copolymers with different molecular weights and block lengths.[21] In that study, the pore size could be tailored, but the pore diameter could not be decreased below the pore diameter of the single-component block copolymer membrane. Moreover, in the previous studies, the pore sizes of the BCP membranes were consistently equal to or larger than 20 nm. Here, we selected blends of interacting AB/AC copolymers and decreased the pore size to the nanofiltration range (smaller than 3 nm). Two di-BCPs, that is, high-molecular-weight polystyrene-*b*-poly(4-vinylpyridine) (PS_{1807}-*b*-$P4VP_{609}$) and low-molecular-weight polystyrene-*b*-poly(acrylic acid) (PS_{144}-*b*-PAA_{22}), in which P4VP and PAA can interact through hydrogen bonds (Supporting Information, Scheme S1), were chosen. Instead of directly patterning the pores, we discovered that nanoscale voids, which give rise to the pores in the blended BCP membrane, are formed spontaneously between the densely packed spherical micelles.

The new blended BCP membranes were fabricated by introducing different amounts of PS_{144}-*b*-PAA_{22} into PS_{1807}-*b*-$P4VP_{609}$/DMF/dioxane/acetone mixtures. The initial PS-*b*-

[*] Dr. H. Z. Yu,[+] Dr. X. Y. Qiu,[+] Prof. K. V. Peinemann
Advanced Membranes and Porous Materials Center
4700 King Abdullah University of Science and Technology (KAUST)
Thuwal 23955-6900 (Kingdom of Saudi Arabia)
E-mail: klausviktor.peinemann@kaust.edu.sa
N. Moreno, Prof. S. P. Nunes
Biological and Environmental Science and Engineering Division (KAUST)
Thuwal 23955-6900 (Kingdom of Saudi Arabia)
N. Moreno, Prof. V. M. Calo
Center for Numerical Porous Media (KAUST)
Thuwal 23955-6900 (Kingdom of Saudi Arabia)
Prof. V. M. Calo
Earth Science and Engineering & Applied Mathematics and Computational Science (KAUST)
Thuwal 23955-6900 (Kingdom of Saudi Arabia)
Dr. Z. W. Ma
School of Optoelectronic Information
Chongqing University of Technology
Chongqing 40054 (China)
[+] These authors contributed equally to this work.

Supporting information for this article is available on the WWW under http://dx.doi.org/10.1002/anie.201505663.

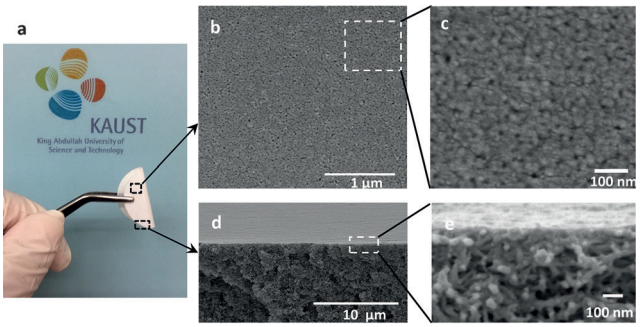

Figure 1. a) Photograph showing the flexibility of the blended BCP PS_{144}-*b*-PAA_{22}/PS_{1807}-*b*-$P4VP_{609}$ membrane with a 6:1 molar ratio. b, c) FESEM images of the membrane surface at different magnifications, showing a large number of small pores. d, e) Cross-section FESEM images showing the thin top layer and the sponge-like bottom layer at different magnifications.

P4VP weight was constant in all experiments, whereas the PS_{144}-*b*-PAA_{22}/PS_{1807}-*b*-$P4VP_{609}$ molar ratio ranged from 2.5:1 to 9:1. A flexible membrane (Figure 1a) was obtained comprising a thin layer on top of a sponge-like layer. The blended BCP membrane with a PS_{144}-*b*-PAA_{22}/PS_{1807}-*b*-$P4VP_{609}$ molar ratio of 6:1 is shown in Figure 1b and 1c; these images suggest a high pore density. The average thickness of the top layer as shown in the cross-section scanning electron microscopy (SEM) images (Figure 1d, e) was only approximately 60 nm. To evaluate the pore size of the blended BCP membranes, we filtered protoporphyrin IX ($M_w = 562.6\ g\,mol^{-1}$, $0.01\ mg\,mL^{-1}$) and lysine ($M_w = 146.2\ g\,mol^{-1}$, $1\ mg\,mL^{-1}$) solutions through the membranes. The membranes were tested in an Amicon stirred cell at a pressure of 1.37 bar. We manufactured membrane areas of $50\ cm^2$ or larger; the final membrane discs for testing had diameters of 2.2 cm.

Figure 2a shows that the retentate concentration of protoporphyrin IX increased with filtration time, and no protoporphyrin IX could be detected in the permeate. This means that water passed through the membrane while protoporphyrin IX was rejected by the blended BCP membrane. However, lysine freely passed through the membrane without rejection. Protoporphyrin IX and lysine have diameters of 1.47 nm and 0.9 nm, respectively (Figure S1), as characterized by DLS,[2] indicating that the effective pore diameter of the blended BCP membrane was smaller than approximately 1.5 nm. Furthermore, Brunauer–Emmett–Teller (BET) analysis, based on the N_2 adsorption isotherm determined using the Barrett–Joyner–Halenda (BJH) method, shows a sharp peak for a pore width of about 1.7 nm (Figure S5) and a broader distribution above 10 nm. The peaks for the membranes were observed to be asymmetric, and the peak in the lower size range is consistent with the sharp cut-off of the membrane's selective layer, whereas the broader distribution in the larger size range corresponds to sub-layers with increasing pore structures formed by macrophase separation. More detailed information on the filtration of different solutes through the membranes is presented in Table S1.

Another remarkable property of this membrane is that the fluxes were as high as $540\ L\,m^{-2}\,h^{-1}$ for the protoporphyrin IX solution and $592\ L\,m^{-2}\,h^{-1}$ for pure water at a pressure of 1.37 bar. Compared with commercial membranes with similar pore sizes, our blended BCP membranes are manufactured using a simple one-step fabrication process; they have a narrow pore size distribution, high water permeability, and high scale-up potential. Furthermore, the water flux through the membrane with the 6:1 PS_{144}-*b*-PAA_{22}/PS_{1807}-*b*-$P4VP_{609}$ molar ratio increased linearly with pressure in the range of 0.5–3.5 bar (Figure 2b), indicating the stability of the membrane.

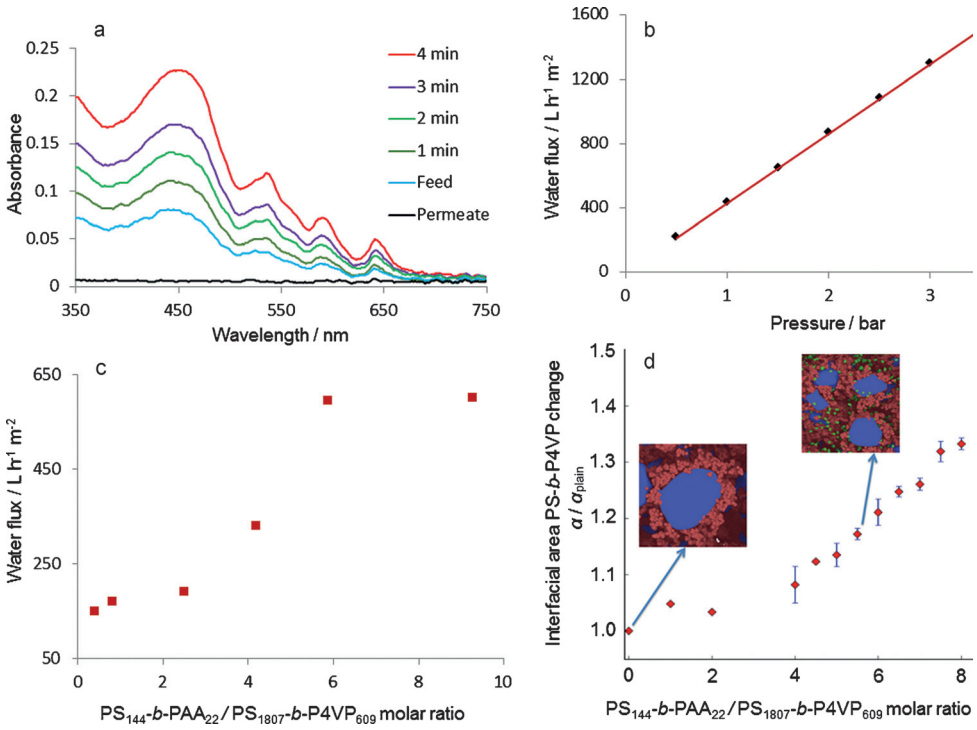

Figure 2. a) UV/Vis absorption spectra show the change in concentration of the aqueous solution of protoporphyrin IX with filtration time and indicate the complete rejection of protoporphyrin IX by the blended BCP membrane with a 6:1 PS_{144}-*b*-PAA_{22}/PS_{1807}-*b*-$P4VP_{609}$ molar ratio. b) Pressure-dependent changes in the pure-water permeability of the blended BCP membrane (6:1 molar ratio). c) The graph shows how the water permeability changes with the content of PS_{144}-*b*-PAA_{22} in the blended BCP membrane. d) Changes in the interfacial area (α) between the PS and P4VP domains with the PS_{144}-*b*-PAA_{22}/PS_{1807}-*b*-$P4VP_{609}$ molar ratio, relative to the plain system.

The formation of nanopores with ultrafast water permeation is guided by the self-assembly of the two copolymer molecules in the solution. A special feature of the plain PS-*b*-P4VP membrane formation in a selective solvent mixture is the micelle formation and its supramolecular assembly in hexagonal order. This order is practically immobilized by immersion in water, a non-solvent for the block copolymer. At the same time, phase separation by spinodal decomposition takes place, leading to the consolidation of a more disordered, asymmetric porous substructure.[14,15] The ordered hexagonal top layer of the plain PS-*b*-P4VP can be seen in Figure 3b, imaged by an atomic force microscope (AFM). We

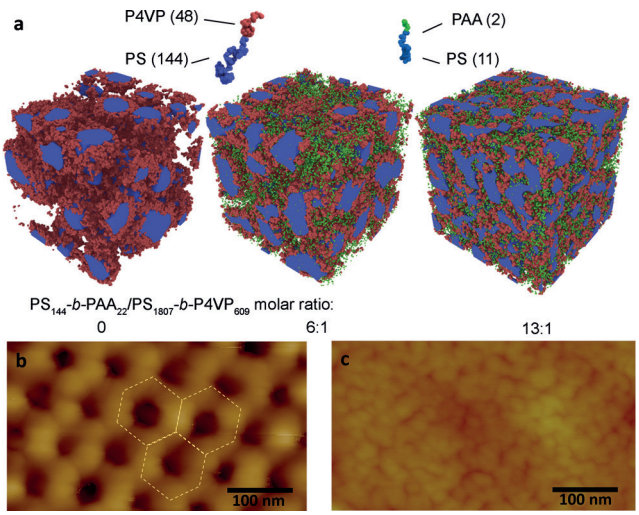

Figure 3. a) Self-assembled structures obtained by computational simulations (DPD), under experimental conditions (17% of PS-*b*-P4VP) with different PS_{144}-*b*-PAA_{22}/PS_{1807}-*b*-$P4VP_{609}$ molar ratios. Solvent particles and PS beads of PS_{144}-*b*-PAA_{22} are omitted for clarity. b, c) AFM images show the surfaces of b) the pure PS_{1807}-*b*-$P4VP_{609}$ membrane and c) the blended BCP membrane with a 6:1 PS_{144}-*b*-PAA_{22}/PS_{1807}-*b*-$P4VP_{609}$ molar ratio. The Figures indicate the morphological transition of the surface from quasi-hexagonal (dashed circles) to densely packed spherical micelles, leading to smaller pores and a higher pore density.

previously investigated the mechanism of pore formation in membranes obtained from single PS-*b*-P4VP copolymers by small-angle X-ray scattering (SAXS),[19] cryo-microscopy,[22,23] and in situ grazing-incidence SAXS[23] and demonstrated how self-assembly in solution is relevant to the process and how it is affected by the copolymer concentration and solvent composition. With the introduction of PS-*b*-PAA to the PS-*b*-P4VP solution, the micellar order is disturbed, and a much denser surface is obtained, as shown in Figure 3c (by AFM) as well as in Figure 1b (by field emission scanning electron microscopy, FESEM). The assembly in solution as well as the final membrane morphology are more complex. Vyhnalkova[24,25] et al. recently reported a detailed investigation of the morphology of PS-*b*-P4VP/PS-*b*-PAA mixtures in relatively diluted solutions containing water. They emphasized the complexity and the interplay between the copolymer lengths as well as the ionic character, solubility, and response to protonation of these mixtures. The solutions that we used for membrane casting were in a much higher concentration range than those used by Vyhnalkova et al.

To understand the assembly changes in the presence of PS-*b*-PAA in the concentration range relevant to membranes, we modeled the block copolymer blends using dissipative particle dynamics (DPD; Figure 4), a method introduced by

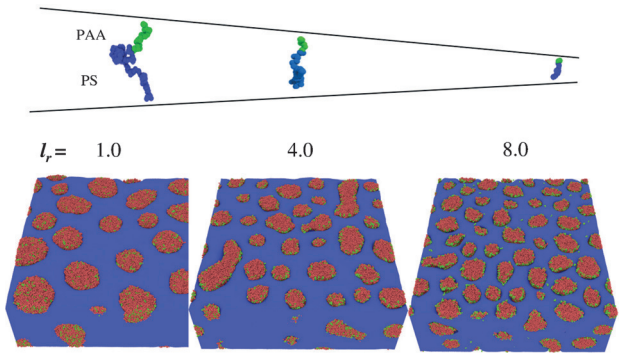

Figure 4. DPD results showing the effect of the length of the PS-*b*-PAA copolymer on the self-assembly morphology in solution. l_r is the length ratio, and $l_r = N_{PS\text{-}b\text{-}P4VP}/N_{PS\text{-}b\text{-}PAA}$. The PS_{1807}-*b*-$P4VP_{609}$ concentration remained constant at 25 wt%, with a molar ratio $n_{PS\text{-}b\text{-}PAA}/n_{PS\text{-}b\text{-}P4VP}$ of 8.6:1. PS blocks are depicted in blue, whereas the red and green domains represent P4VP and PAA segments, respectively. Solvent particles are omitted for clarity. As the l_r value increases, the PS-*b*-PAA is preferentially localized at the interface.

Hoogerbrugge and Koelman.[26] We previously used DPD simulations to explain the formation of plain PS-*b*-P4VP membranes.[22] Whereas PS_{1807}-*b*-$P4VP_{609}$ formed micelles in the solvent mixture investigated (DMF/dioxane/acetone), the segregation was not strong in the case of pure PS_{144}-*b*-PAA_{22} owing to the relatively low AA block size. Segregation is favored when the thermodynamic interactions multiplied by the block sizes are high (Figure S2 and Tables S3–S5). When the two copolymers are mixed, complexes are formed owing to hydrogen-bonding interactions,[27] and the PAA blocks can penetrate the shell of the PS-*b*-P4VP micelles, leading to the morphology changes depicted in Figures 3a and S3. The DPD simulation shows that the radius of gyration for the PS-*b*-P4VP chains decreased as the PS-*b*-PAA ratio increased, as did the characteristic segregation domain size in the final structured membrane (Figure 3a). Correspondingly, the AFM results indicate a decrease in the micellar size from approximately 35 nm for the pure PS-*b*-P4VP membrane (Figure 3b) to about 15 nm or less for the blended BCP membrane (Figure 3c). Smaller pores are thus formed. Conversely, because of the hydrophobic character (PS blocks) of PS-*b*-PAA, we believe that they promote the morphological transition by inserting their hydrophobic chains into the PS-*b*-P4VP micellar aggregates (Figure S3), also leading to an increase in the entropic constraint.[28] A morphological transition from quasi-hexagonal to densely packed spherical micelles also helps to relieve this entropy strain (Figure 3), leading to smaller, highly dense pores. The final surface morphology is the result of cooperation between these two factors, that is, hydrogen bonding between the P4VP and PAA units and the hydrophobic tails of PS-*b*-PAA

inserting into the PS-*b*-P4VP micellar cores. The clear change in the water flux as the relative amount of PS-*b*-PAA is increased is shown in Figure 2c. The block length of PS-*b*-PAA also plays a critical role in the fabrication of the blended membrane. Aggregation is likely to happen in blends of PS_{1807}-*b*-$P4VP_{609}$ and large-molecular-weight PS_{673}-*b*-PAA_{180} as confirmed both by experimental (not shown here) and simulation results (Figures 4, S3, and S4). The effect of the length ratio ($l_r = N_{PS\text{-}b\text{-}P4VP}/N_{PS\text{-}b\text{-}PAA}$) on the overall self-assembly is evident in the DPD results depicted in Figure 4. Lower values of l_r correspond to longer PAA chains and lead to strong associations with P4VP domains and an overall increase in the domain size. The morphology after the concentration of the polymer has been increased by solvent evaporation and the addition of water (a poor solvent in this case) to the system is simulated in Figure 4b, demonstrating the formation of a large number of smaller domains in the presence of small PS-*b*-PAA copolymers. These domains give rise to the membrane's pores.

The faster water transport through the blended BCP membrane (Figure 2c and Table S1) is a consequence of the exceptional pore density, the thin top layer, and the highly hydrophilic PAA blocks. The number of pores increases dramatically after the addition of PS-*b*-PAA (Figure 3b,c), which is partially located in the pore walls. A clear transition in the permeability characteristics is seen for PS_{144}-*b*-PAA_{22}/PS_{1807}-*b*-$P4VP_{609}$ molar ratios between 4:1 and 6:1. The increase in hydrophilicity is confirmed by the contact angle values and the water membrane adhesion (Table S2). The transition in permeability can also be associated with the reduction in micellar size. This trend is consistent with the increment in the interfacial area (α) between the PS and P4VP domains measured in our simulations (Figure 2c). The abrupt change in area at molar ratios around 4:1 reflects the reduction in the characteristic domain size.

The advantage of this technique is that the fabrication of the nanoporous membrane is simple compared with post-deposition fabrication processes[13,29,30] and the synthesis of new polymers.[31] Our simulations suggest that a variety of copolymers can be used with this technique. It should also be possible to scale-up the blended BCP membrane fabrication process by combining high separation factors with high fluxes.

Experimental Section

Membrane preparation: The polystyrene-*b*-poly(4-vinylpyridine) (PS_{1807}-*b*-$P4VP_{609}$, $M_n = 252\,000\ g\,mol^{-1}$) and polystyrene-*b*-poly(acrylic acid) block copolymers (PS_{144}-*b*-PAA_{22}, $M_n = 16\,600\ g\,mol^{-1}$ and PS_{673}-*b*-PAA_{180}, $M_n = 83\,000\ g\,mol^{-1}$) were purchased from Polymer Source, Inc., Canada. The subscripts indicate the number of repeating units in the blocks. All other chemicals were supplied by Aldrich. The blended BCP membranes were cast from a polymer solution mixture of PS_{144}-*b*-PAA_{22} and PS_{1807}-*b*-$P4VP_{609}$/DMF/dioxane/acetone on a Hirose TH100 polyester support, using casting blades with 200 μm gaps. The PS_{1807}-*b*-$P4VP_{609}$ weight and the organic solvent composition remained constant at 18 wt% copolymer, 24 wt% *N*,*N*-dimethyl formamide (DMF), 42 wt% dioxane, and 16 wt% acetone for both the blended BCP membrane and the plain PS-*b*-P4VP membrane, whereas the molar ratio ($n_{PS\text{-}b\text{-}PAA}/n_{PS\text{-}b\text{-}P4VP}$) of PS_{144}-*b*-PAA_{22} to PS_{1807}-*b*-$P4VP_{609}$ ranged from 2.5:1 to 9:1 in the blended BCP membrane. The solvent was allowed to evaporate for up to 10 s at room temperature, and the film was then immersed in a non-solvent bath (Milli-Q water, 18.2 MΩ) at room temperature.

Field emission scanning electron microscopy (FESEM) images were obtained using an FEI Quanta 600 series microscope at 5 kV with a working distance of 10 mm. Atomic force microscopy (AFM) images were obtained on an ICON Veeco microscope operating in the tapping mode using commercial silicon TM AFM tips (model MPP 12100). Additional details for the characterization of the membranes, including contact angle, BET, and DLS analyses, are described in the Supporting Information. The water flux measurements as well as the structures and sizes of the molecules for the rejection experiment are also explained in the Supporting Information. The rejection of dyes, proteins, and gold particles was monitored by a NanoDrop 2000/2000c spectrophotometer (Thermo Fisher Scientific).

Dissipative particle dynamics (DPD) simulations**:** The DPD simulations were conducted in a large-scale atomic/molecular massively parallel simulator (LAMMPS).[32] We used the standard DPD units of length ($r_c = 1$), mass ($m = 1$), energy ($\varepsilon = k_B T = 1$), and time ($\tau = 1$). The particle density in our system was $\rho_n = 3$ particles per r_c^3. A time step of 0.04τ was used to restrict temperature fluctuations to be smaller than 1%. The simulated systems were evolved for 10^6 time steps. The analysis and visualization of the computational results were performed with in-house software and OVITO.[33,34] We used periodic boundary conditions in cubic simulation boxes of the size $L_{box} = 131 r_c$. The box size was defined to be proportional to the overestimated radius of gyration as $L_{box} = z\, r_o N^{\upsilon}_{PS\text{-}b\text{-}P4VP}$, where $z = 6$ is the proportionality constant, $r_o = 0.8 r_c$ is the equilibrium bond length between connected particles, $N_{PS\text{-}b\text{-}P4VP} = 192$, and $\upsilon = 0.63$. The value of υ is an overestimated parameter, as we defined the box size as if the polymer coils were extended. Detailed parameters and descriptions are provided in the Supporting Information.

Acknowledgements

We gratefully acknowledge financial support from the King Abdullah University of Science and Technology (KAUST) with special thanks for partial funding from the KAUST CRG2 project "Charge-mosaic and Block Copolymer Membranes". We also thank Dr. Omar El Tall from the Analytical Core Lab at KAUST for help with the BET analysis. N.M. and V.C. acknowledge support from the Texas Advanced Computing Center (TACC) at the University of Texas at Austin and the KAUST research computing center for providing HPC resources to perform the simulations and their excellent technical support. Z.M. thanks the National Natural Science Foundation of China (21304110).

Keywords: block copolymers · membranes · nanofiltration · self-assembly

How to cite: *Angew. Chem. Int. Ed.* **2015**, *54*, 13937–13941
Angew. Chem. **2015**, *127*, 14143–14147

[1] L. A. Baker, S. P. Bird, *Nat. Nanotechnol.* **2008**, *3*, 73–74.
[2] X. Peng, J. Jin, Y. Nakamura, T. Ohno, I. Ichinose, *Nat. Nanotechnol.* **2009**, *4*, 353–357.
[3] C. C. Striemer, T. R. Gaborski, J. McGrath, P. M. Fauchet, *Nature* **2007**, *445*, 749–753.
[4] S. Karan, S. Samitse, X. Peng, K. Kurashima, I. Ichiinose, *Science* **2012**, *335*, 444–447.
[5] E. Krieg, H. Weissman, E. Shirman, E. Shimoni, B. Rybtchinski, *Nat. Nanotechnol.* **2011**, *6*, 141–146.

[6] W. Lee, R. Ji, U. Gösele, K. Nielsch, *Nat. Mater.* **2006**, *5*, 741 – 747.
[7] G. M. Whitesides, B. Grzybowski, *Science* **2002**, *295*, 2418 – 2421.
[8] A. Ruzette, L. Leibler, *Nat. Mater.* **2005**, *4*, 19 – 31.
[9] F. S. Bates, G. H. Fredrickson, *Phys. Today* **1999**, *52*, 32 – 38.
[10] E. A. Jackson, M. A. Hillmyer, *ACS Nano* **2010**, *4*, 3548 – 3553.
[11] J. Bang, U. Jeong, D. Y. Ryu, T. P. Russell, C. J. Hawker, *Adv. Mater.* **2009**, *21*, 4769 – 4792.
[12] K.-V. Peinemann, V. Abetz, P. F. W. Simon, *Nat. Mater.* **2007**, *6*, 992 – 996.
[13] H. Yu, X. Qiu, S. P. Nunes, K.-V. Peinemann, *Angew. Chem. Int. Ed.* **2014**, *53*, 10072 – 10076; *Angew. Chem.* **2014**, *126*, 10236 – 10240
[14] S. P. Nunes, R. Sougrat, B. Hooghan, D. H. Anjum, A. R. Behzad, L. Zhao, N. Pradeep, I. Pinnau, U. Vainio, K.-V. Peinemann, *Macromolecules* **2010**, *43*, 8079 – 8085.
[15] S. P. Nunes, M. Karunakaran, N. Pradeep, A. R. Behzad, B. Hooghan, R. Sougrat, H. He, K.-V. Peinemann, *Langmuir* **2011**, *27*, 10184 – 10190.
[16] W. Park, Y. Kim, J. Jeong, K. Kim, J.-K. Yoo, Y. Hur, J. Kim, E. L. Thomas, A. Alexander-Katz, Y. S. Jung, *Sci. Rep.* **2013**, *3*, 3190.
[17] M. Stoykovich, M. Müller, S. O. Kim, H. H. Solak, E. W. Edwards, J. J. de Pablo, P. F. Nealey, *Science* **2005**, *308*, 1442 – 1446.
[18] C. Tang, E. M. Lennon, G. H. Fredrickson, E. J. Kramer, C. J. Hawker, *Science* **2008**, *322*, 429 – 432.
[19] D. A. Christian, W. Tian, W. G. Ellenbroek, I. Levental, K. Rajagopal, P. A. Janmey, A. J. Liu, T. Baumgart, D. E. Discher, *Nat. Mater.* **2009**, *8*, 843 – 849.
[20] J. Zhu, S. Zhang, K. Zhang, X. Wang, J. W. Mays, K. L. Wooley, D. J. Pochan, *Nat. Commun.* **2013**, *4*, 2297.
[21] M. Radjabian, V. Abetz, *Adv. Mater.* **2015**, *27*, 352 – 355.
[22] D. S. Marques, U. Vainio, N. M. Chaparro, V. M. Calo, A. R. Bezahd, J. W. Pitera, K.-V. Peinemann, S. P. Nunes, *Soft Matter* **2013**, *9*, 5557 – 5564.
[23] D. S. Marques, R. M. Dorin, U. Wiesner, D.-M. Smilgies, A. R. Behzad, U. Vainio, K.-V. Peinemann, S. P. Nunes, *Polymer* **2014**, *55*, 1327 – 1332.
[24] R. Vyhnalkova, A. H. Müller, A. Eisenberg, *Langmuir* **2014**, *30*, 13152 – 13163.
[25] R. Vyhnalkova, A. H. Müller, A. Eisenberg, *Langmuir* **2014**, *30*, 5031 – 5040.
[26] P. J. Hoogerbrugge, J. M. V. A. Koelman, *Europhys. Lett.* **1992**, *19*, 155 – 160.
[27] W. Zhang, L. Shi, Y. An, K. Wu, L. Gao, Z. Liu, R. Ma, Q. Meng, C. Zhao, B. He, *Macromolecules* **2004**, *37*, 2924 – 2929.
[28] N. S. Cameron, M. K. Corbierre, A. Eisenberg, *Can. J. Chem.* **1999**, *77*, 1311 – 1326.
[29] P. Chen, T. Mitsui, D. Farmer, J. Golovchenko, R. G. Gordon, D. Branton, *Nano Lett.* **2004**, *4*, 1333 – 1337.
[30] D. Losic, G. Triani, P. J. Evans, A. Atanacio, J. G. Mitchell, N. H. Voelcker, *J. Mater. Chem.* **2006**, *16*, 4029 – 4034.
[31] M. Barsbay, O. Güven, H. Bessbousse, T. L. Wade, F. Beuneu, M.-C. Clochard, *J. Membr. Sci.* **2013**, *445*, 135 – 145.
[32] S. Plimpton, *J. Comput. Phys.* **1995**, *117*, 1 – 19.
[33] A. Stukowski, *Modell. Simul. Mater. Sci. Eng.* **2010**, *18*, 015012.
[34] A. Stukowski, *JOM* **2013**, *66*, 399 – 407.

Received: June 19, 2015
Published online: September 21, 2015

